Crustal structure of the India–Asia collision zone, southern Tibet, from INDEPTH MT investigations[☆]

Jessica E. Spratt[a,b,1], Alan G. Jones[a,b,*,1], K. Douglas Nelson[a,2], Martyn J. Unsworth[c]

INDEPTH MT Team[3]

[a] *Department of Earth Sciences, Syracuse University, Syracuse, New York, NY 13244, USA*
[b] *Geological Survey of Canada, 615 Booth St., Ottawa, Ont., Canada K1A 0E9*
[c] *Department of Physics, University of Alberta, Edmonton, Alta., Canada T6G 2J1*

K. Douglas Nelson passed away unexpectedly on August 17, 2002. Doug was a true visionary who led the INDEPTH project with drive, insight and humour. JES was Doug's graduate student at the time of his death. Doug was an inspiration to us all. We dedicate this paper in Doug's memory.

Abstract

Project INDEPTH was initiated in 1992 to develop a better understanding of the deep structure and mechanics of the Himalaya-Tibet region, and magnetotelluric surveying was added during INDEPTH Phase II in 1995. Broadband and long period data were acquired in 1995 along a N–S transect crossing the India–Asia collision zone, the Yarlung-Zangbo suture, at ∼90°E longitude. However, these data failed to penetrate to the deep crustal and mantle depths due to low solar activity, and the presence of the thick conductive crust. Deep crustal and upper mantle information is key to test the model of subcretion to southern Tibet by the stiff Indian mantle lid. In order to try to obtain such information, and to test along-strike variability of the Yarlung-Zangbo suture zone, a magnetotelluric experiment was performed in 2001 roughly along longitude 92°E, containing an ultra-long period component. MT data were acquired at 28 locations along the new profile, with long period data at 15 of these, and ultra-long period data at five of these 15. Initial comparisons of the models generated from the 1996 and 2001 datasets indicate little variation in electrical conductivity structure along-strike.
© 2004 Published by Elsevier B.V.

Keywords: India–Asia collision; Tethyan closure; Tibetan Plateau; INDEPTH; Electromagnetic induction; Magnetotelluric technique

1. Introduction

The collision of the Indian subcontinent with Asia is unparalleled – it offers the holy grail for interpreting the cryptic rock record of ancient collisional orogens and provides a benchmark for testing evolutionary theories of tectonic processes. Despite its importance, it remains poorly studied to this day due to the isolation of the Tibetan Plateau. Continent–continent collision between India and Asia, which formed the Himalayan mountain range and the Tibetan Plateau, began about 55 Ma and continues to the present (Besse and Courtillot, 1988). Both the Himalaya and adjacent Tibetan Plateau have reached an average elevation of about 5 km with an average crustal thickness of about 70 km (Molnar et al., 1993). The crust underlying the Tibetan Plateau is comprised of several continental fragments that were progressively accreted to the southern margin of Asia during late Paleozoic through Mesozoic times, and separated by ophiolitic suture zones (Yin and Harrison, 2000). The Yarlung-Zangbo suture (YZS), lying just north of the Himalaya in southern Tibet, marks the paleogeographic boundary between what was Indian crust and what was Asian crust prior to initiation of collision. This is a key region for

determining whether or not Indian lithospheric mantle is being subducted beneath southern Tibet. Secondly, determining the nature and distribution of fluids within the lithosphere in active plate boundary zones is crucial for the understanding of the mechanics of orogeny, as the presence of fluids within rocks can dramatically alter their rheology (Mei and Kohlstedt, 2000). The magnetotelluric method (MT), which makes use of naturally occurring electric currents within the Earth, is particularly useful in determining the presence and distribution of fluids to substantial depths within the lithosphere (see, e.g., Jones, 1992, 1993).

Since 1992 Project INDEPTH (International Deep Profiling of Tibet and the Himalaya) has been collecting geophysical and geological data in Tibet to study the nature and structure of the lithosphere beneath this region (Zhao and Nelson, 1993; Nelson et al., 1996). There have been a total of three major field campaigns (INDEPTHs I–III) completed to date, during which seismological, electromagnetic and geological data have been acquired along a series of north–south trending profiles. In total the INDEPTH lines comprise a discontinuous transect from the crest of the Himalaya to the Kunlun fault in the northern interior of the Tibetan Plateau (Fig. 1).
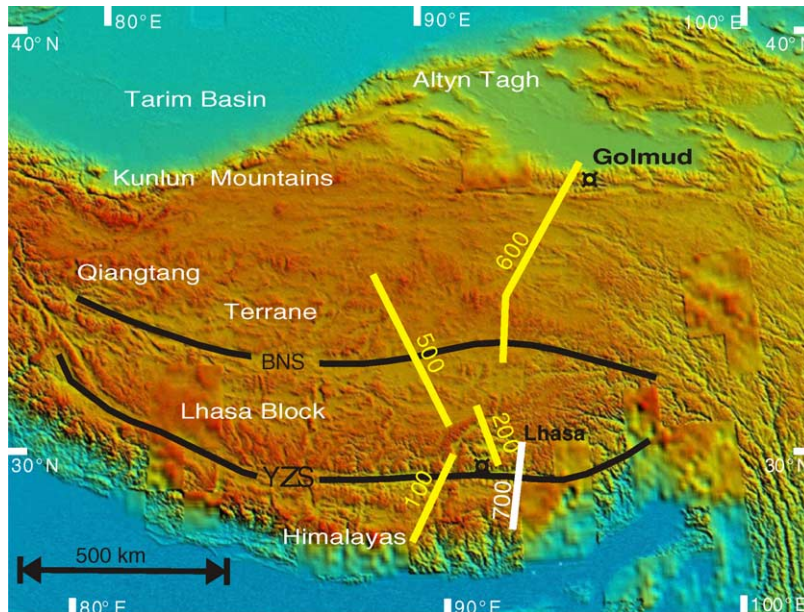

Fig. 1. Project INDEPTH's magnetotelluric profiles across the Tibetan Plateau. The 700-line in white is the profile recorded during the 2001 summer field season.

Electromagnetic acquisition, using the natural-source magnetotelluric (MT) technique, was added during INDEPTH-II and was also undertaken in INDEPTH–III. Both broadband (BBMT) and long period (LMT) magnetotelluric (MT) data were acquired to determine the electrical resistivity structure of the Tibetan Plateau crust and uppermost mantle, and to complement the geological and seismological studies. To date, INDEPTH has collected ∼1600 km of MT data that extend from southern Tibet to the northern edge of the Tibetan Plateau (Fig. 1). These MT data have revealed anomalously high electrical conductivity pervasively throughout the middle to lower crust across the entire Tibetan Plateau (Wei et al., 2001). The enhanced conductivity zone has been interpreted to represent partial melting in the crust with the possible presence of accompanying hydrothermal fluids (Nelson et al., 1996; Brown et al., 1996; Chen et al., 1996; Wei et al., 2001; Li et al., 2003).

In 1995, as part of INDEPTH-II, BBMT and LMT data were acquired along a N–S 100-line transect crossing the YZS at ∼90°E longitude (Chen et al., 1996). However, these data failed to penetrate to the deep crustal and mantle depths due to

(1) sunspot activity was at its lowest in the last 11-year solar cycle,
(2) Tibetan crust is double-thickened, with Moho depth estimates of >70 km, and
(3) crustal conductivity is high at depths below about 20 km, and penetration beyond ∼40 km was not possible. The skin depth phenomenon of electromagnetic fields (e.g., Jones, 1999) results in high attenuation of the fields as they pass through conducting structures.

Deep crustal and uppermost mantle information is key to determining whether the subcretion of Indian mantle lithosphere is occurring. In the 2001 summer field season, new MT data were acquired along a second
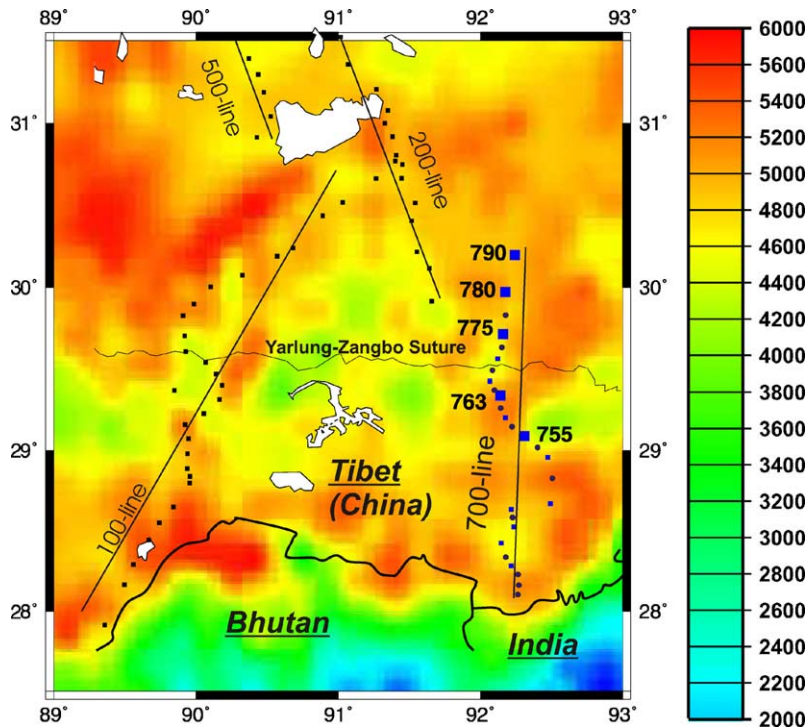

Fig. 2. Map of the MT site locations across the Yarlung-Zangbo suture zone in Southern Tibet. The 100-line and the 200-line are MT data collected as part of INDEPTH II. The broadband sites are shown as blue circles, the broadband and long period sites are blue squares and the extra long period sites are shown as larger blue squares within the 700-line profile. The coloured background represents the average surface elevation.

N–S profile, the 700-line, crossing the Yarlung-Zangbo suture (YZS) at 92°E longitude, allowing for the comparison of the conductivity structure along geoelectric strike. At selected sites at the north end of the profile, additional ultra-long period data (>30,000 s) were collected in the hope of sensing deeper beneath the observed mid-crustal high conductivity zone. This paper presents the first results of our analyses and modelling of the new data, and compares the best-fitting model with a new model derived for the 100-line data using the same inversion parameters as for the 700-line data.

2. MT data acquisition

The 700-line MT profile extends for approximately 300 km from just north of the Indian border (the state of Arunachal Pradesh) where it abuts Bhutan and includes 28 BBMT recording stations and 15 LMT sites merged with every other BBMT site (Fig. 2). At each of the 28 MT site locations five components of the time-varying electromagnetic fields were recorded (E_x, E_y, H_x, H_y, and H_z). Acquisition at the BBMT-only sites used EMIs MT-24 instruments, and recorded data in the period range of 0.004–1000 s. At each BBMT + LMT site, data were collected using EMIs equipment (for the BBMT range) and Phoenix LRMT (long range magnetotelluric) instruments (in the LMT range), to yield a total period range of observation of 0.004–30,000 s.

At five sites in the northern half of the profile (755, 763, 775, 780 and 790, Fig. 2), termed ultra-long period (ULMT) sites, an effort was made to acquire natural time variations with periods greater than 30,000 s by switching off the two 30,000 s high-pass filters on the telluric channels within the recording box and by lengthening the distance of the electric dipoles, from 100 m to up to 450 m, to enhance the signal to noise ratio. These sites were left in place for several months (July–August, 2001) subsequent to the main acquisition phase in an attempt to record adequate amounts of ultra-long period data to reveal the conductivity structure beneath the zone of enhanced conductivity. Our endeavour to image deeper was additionally facilitated by the fact that the summer of 2001 coincided with the peak in the 11-year sun spot cycle. This enhances the intensity of the measurable induced currents and allows for better long period data quality over a shorter period of time. Fig. 3 shows an example of improved data
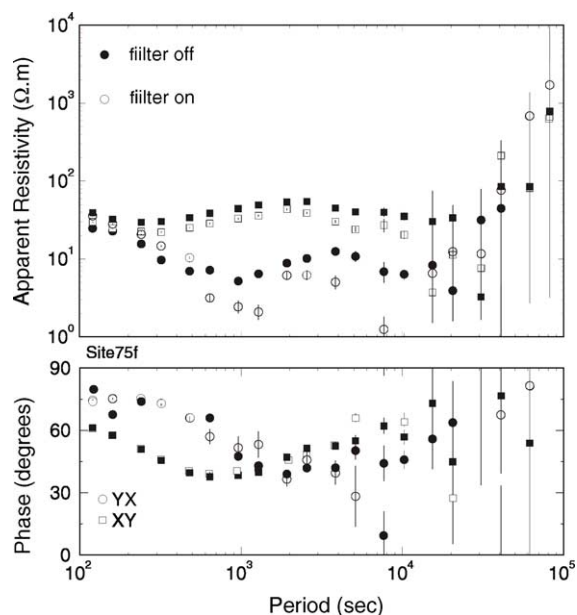

Fig. 3. Response functions for filtered (open symbols) vs. unfiltered (full symbols) data at site 755 showing improved data quality at longer periods. The squares represent the XY data, which is approximately perpendicular to geoelectric strike, and the circles represent the YX data, or approximately parallel to strike.

quality at periods greater that 10,000 s after turning off the extra long period filter. Visual improvement is readily apparent, particularly in the YX estimates between 1000 and 10,000 s, and in the general stability and lack of scatter of the "filter off" estimates compared to the "filter on" ones.

Unfortunately, several problems were encountered during acquisition of the ultra-long period data that resulted in poorer data quality than anticipated. The batteries purchased in Lhasa were of very poor quality and, even with the assistance of solar panels, many failed to keep the systems recording continuously between service checks. Due to the rugged terrain, choice of site location was limited, and many sites were placed in regions with extremely coarse dry soil conditions. In those cases the salt solution of the electrodes often dried out between services, resulting in high electrode noise. Site 780 flooded on two occasions and little data were recovered from it. The most frustrating problem was the inability to download the data from some of the recording boxes after the final service check. Upon retrieving the five ULMT instruments, after 1.5 months

of recording, data from only two sites (790 and 775, Fig. 2) were fully recoverable.

3. Processing, analysis and quality appraisal

For the LMT data, remote reference processing (Gamble et al., 1979) was applied to the data, to reduce the effects of local noise, using the multi-remote reference robust code of Jones (based on Jones and Jödicke, 1984, method 6 in Jones et al., 1989) to yield MT and vertical field geomagnetic transfer function (GTF) response estimates for each site. The quality of the phase

and apparent resistivity response curves for each of the ultra-long period sites (with the exception of site 780) is high to periods of nearly 10,000 s. Fig. 4 shows the response curves for these sites, two of which (755 and 763) lie south of the YZS and two (775 and 790) to the north, in the geographic co-ordinate system. Initial observations of the response curves indicate that site 763 appears to show conductivity at depth (particularly in the RXY, or TM, mode) where 755 clearly indicates a more resistive structure at depth.

The McNeice and Jones (2001) distortion decomposition code was used on the MT responses from each of the sites in the 700-line profile to analyze the
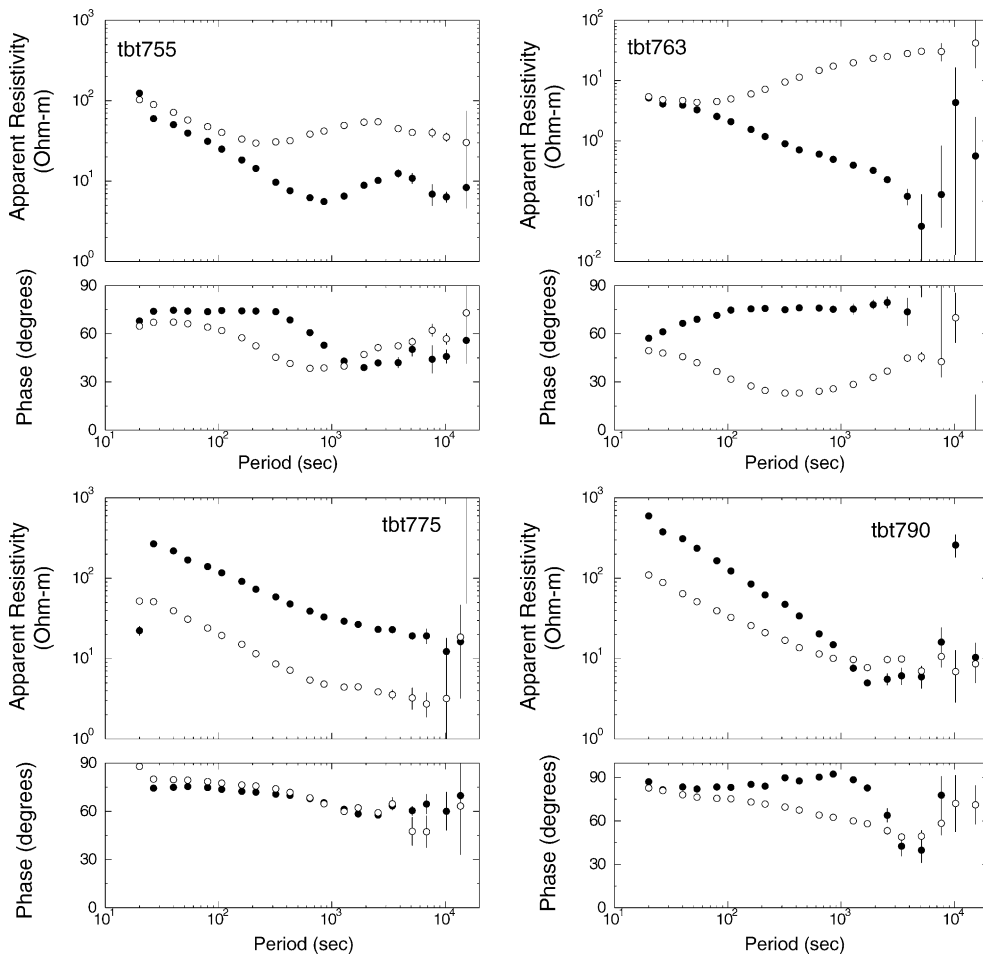

Fig. 4. Magnetotelluric phase and resistivity curves derived from extra long period sites (755, 763, 755, and 790) along the 700-line profile. The open circles represent the YX data, which is approximately perpendicular to geoelectric strike, and the closed circles show the XY data, or approximately parallel to strike.
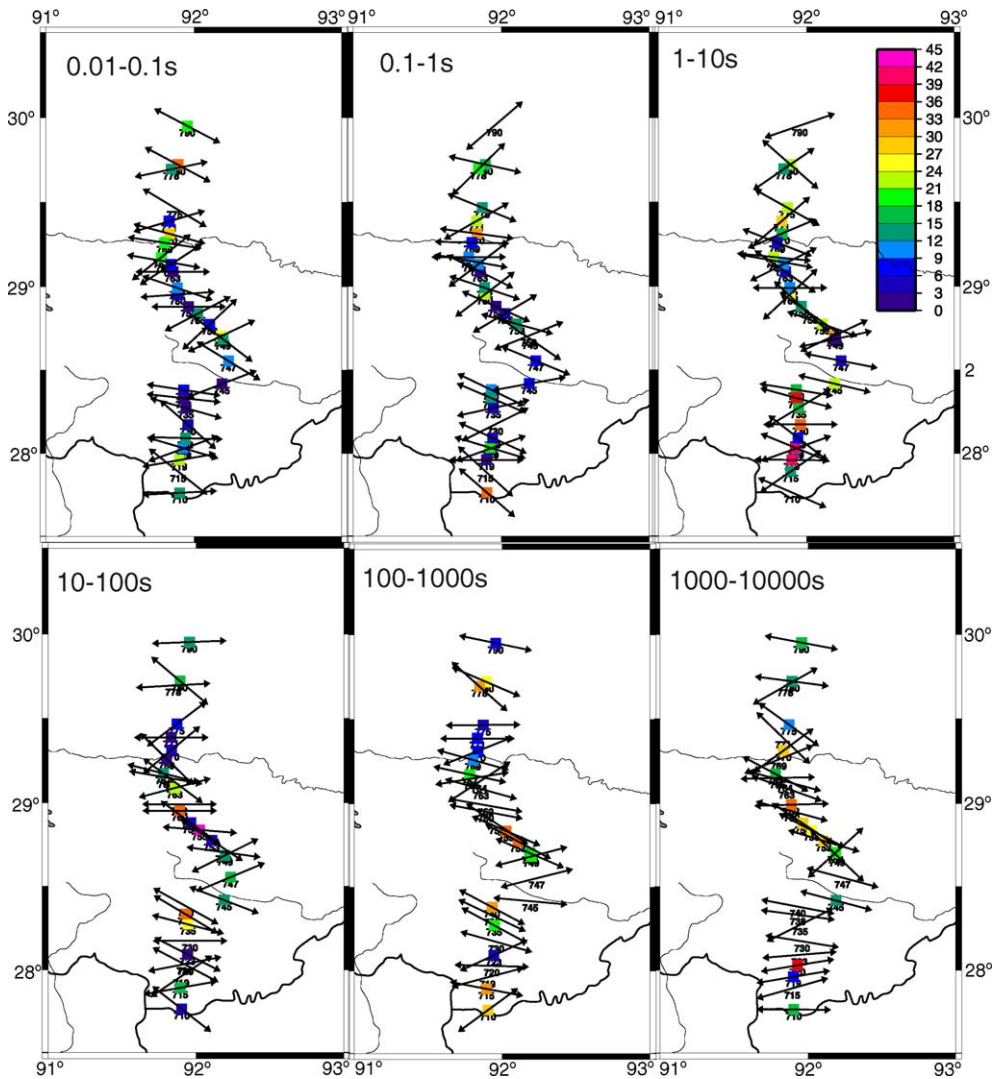
Fig. 5. The unconstrained Groom-Bailey strike decompositions from six period bands. The azimuth of the arrows illustrates the preferred geoelectric strike direction for that period band. The colour index represents the average phase difference between the TM and TE modes, where brighter colours indicate a stronger degree of dimensionality (either intrinsic or structural anisotropy).

responses for galvanic distortions and determine the most accurate geoelectric strike direction. This code is a multi-site, multi-frequency extension of the Groom and Bailey (1989) approach. The strike azimuth from single site decompositions are shown in Fig. 5 for one-decade wide bandwidths from 0.01 to 10,000 s, as well as the average phase difference over the decade between the conductive (strike) and resistive directions. Most of the sites on the profile show consistent azimuth directions

in the period range of 10–10,000 s. Multi-site decompositions were attempted with two and three sites per group, as well as by dividing the profile into three sections (south, middle, and north), over one-decade frequency ranges. The strike azimuth results for the various groupings consistently reveal angles in the range of 106–120°. Based on consistencies and associated errors, two strike angles were consistently found to fit the responses from most of the sites along profile, and

were chosen for interpretation. Single-site, frequency-independent decompositions were performed on each of the MT sites along profile at strike angles of both 108° and 117°, in order to determine the most accurate regional 2-D impedances and observe the associated twist and shear galvanic distortion parameters at each site. Each site was corrected for anisotropy by coalescing apparent resistivity curves between the two orthogonal components to their geometric mean at the highest frequencies.

Subsequently, the distortion-corrected regional response estimates from each site were tested for internal consistency of the phase and resistivity curves by predicting one from the other using Parker and Booker's (1996) *Rhoplus* algorithm. A consistency test based on the dispersion relationships was advocated by Berdichevsky (1999, p. 351). The predicted responses were compared with the observed ones as an aid to determining which responses for each site should be included in the subsequent inversion. Fig. 6 shows examples of this comparison at two BBMT + LMT sites from the 700-line profile. The consistency of predicted (open symbols) versus observed (full symbols) apparent resistivity and phase curves for site 745 is excellent for periods up to 500 s in the TE mode (circles) and up to 2000 s in the TM mode (squares). In contrast, the consistency for site 720 is only good to a period of 4 s for the TE mode, but in the TM mode the Rhoplus test shows that, aside from poor data quality between 4 and

20 s, the data are internally consistent, therefore usable, to long periods (3500 s).

This Rhoplus consistency test is only formally correct for a minimum-phase system, i.e., that the magnitudes and phases are related by Hilbert transformation, which is true of MT 1-D responses (Weidelt, 1972) and the TM-mode responses for a 2-D Earth (Weidelt and Kaikkonen, 1994). However, TE-mode responses that violate this condition are thought to be rare. As a caution though, these conditions are violated for 3-D Earth models, especially those with 3-D local galvanic distortion of regional 2-D Earths (Berdichevsky and Pokhotelov, 1997; Berdichevsky, 1999). Thus, this consistency test must be applied after removal of the effects of galvanic distortion.

4. Preliminary models

Different models were derived using three sets of MT responses; the original uncorrected responses in geographic co-ordinates, the distortion-corrected responses at a strike angle of 117°, and the distortion-corrected responses at a strike angle of 108°. For each of these three sets, inversions were run using the TM data alone (Fig. 7a), the TM and GTF data together (Fig. 7b), the TM and TE data together (Fig. 7c), and finally including the TM, TE and GTF data (Fig. 7d). The responses were inverted using Rodi and Mackie's
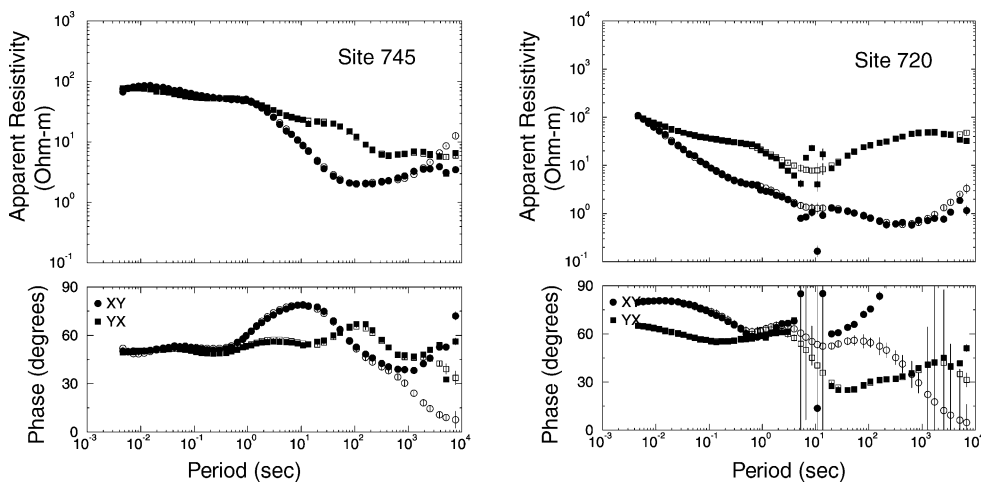

Fig. 6. Phase and resistivity plots with increasing period for two sites along the 700-line profile. The XY curves are the responses in the TE modes and the YX in the TM mode. The open symbols represent data predicted using Rhoplus and the full symbols are the observed data.
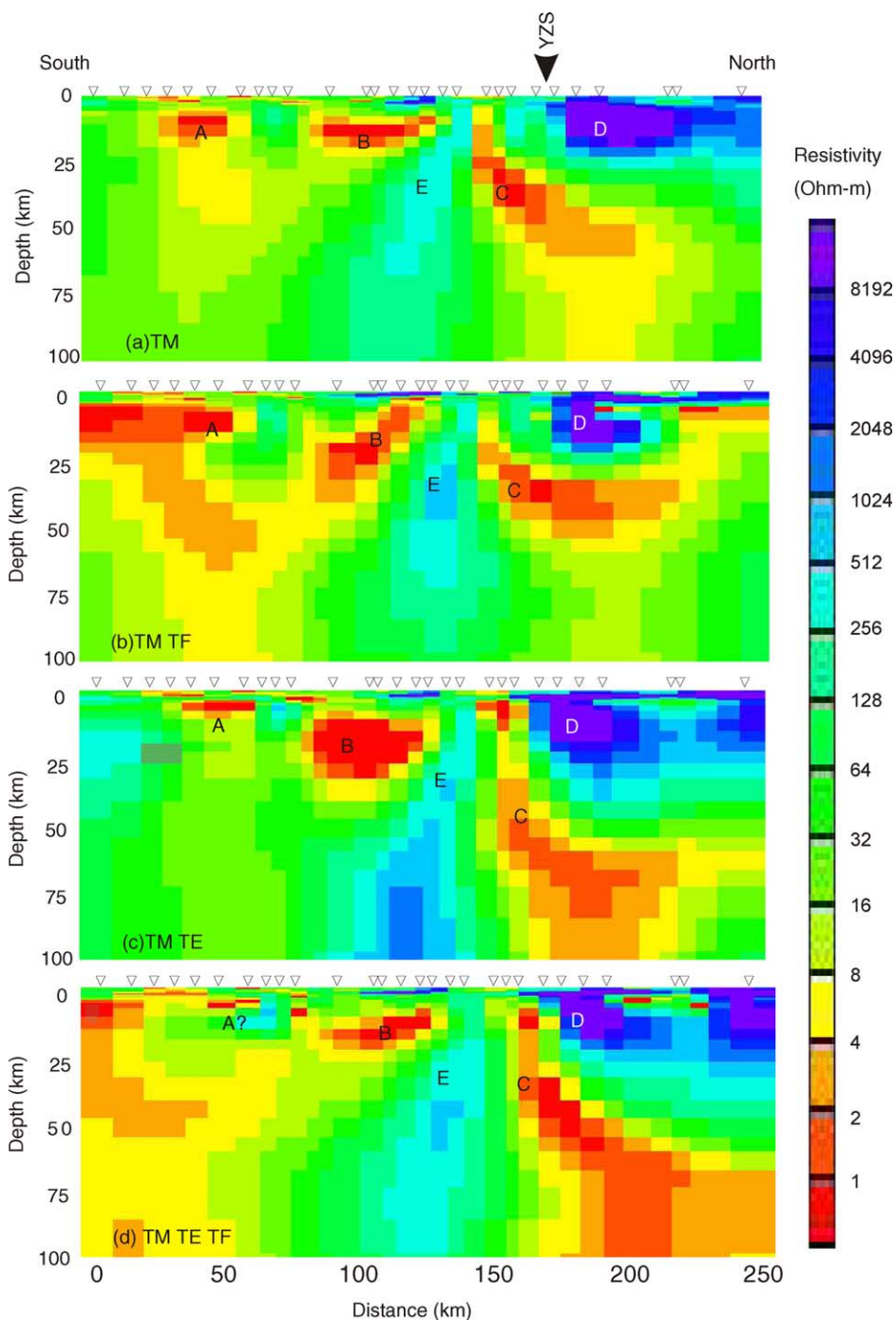
Fig. 7. Inversion models for the 700-line MT data, using Groom-Bailey responses at a strike angle of 108°. (a) Model is derived from inversions of TM data only, with an RMS misfit of 1.9. (b) Model is derived from inversions of both TM and transfer function data and has an RMS misfit of 3.5. (c) Model is derived from inversions of both TM and TE data and has an RMS misfit of 3.6. (d) Model is derived from TM, TE and transfer function data and has an RMS misfit of 4.4. The features A–E represent different structures consistent in each of the models.
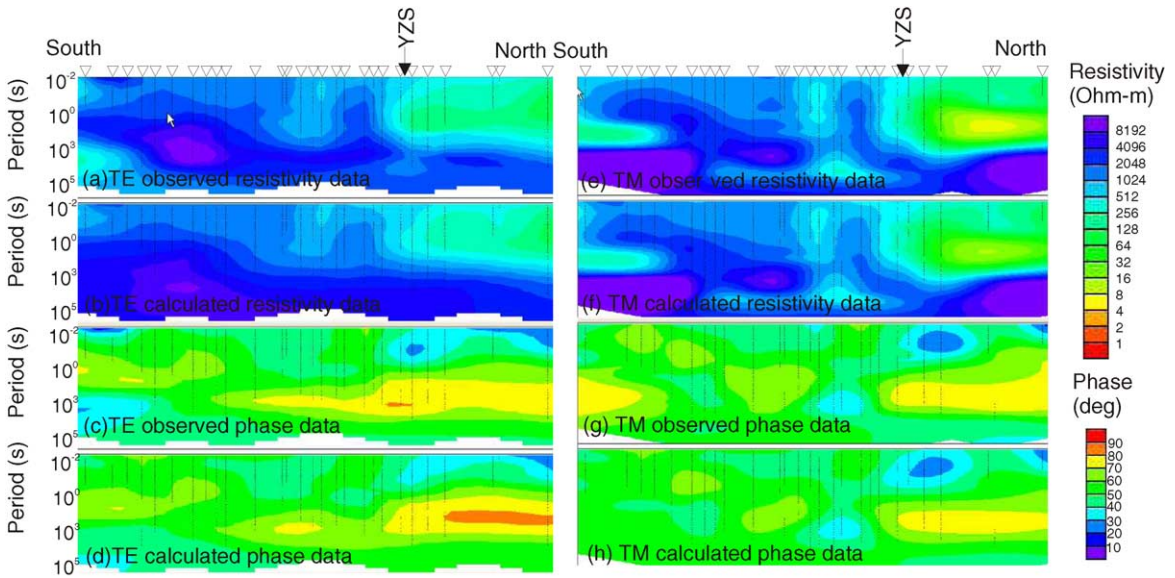
Fig. 8. Pseudosections for abserved responses and the forward calculated response from the TM, TE and GTF model in Fig. 7d. (a–d) The resistivity and phase pseudosections for data in the TE mode. (e–f) The resistivity and phase pseudosections for data in the TM mode.

(2001) RLM2DI code, as implemented in Geosystem's WinGLink interpretation package. The phases were set with a 2° error floor, determined from the acceptable misfit values obtained in the distortion analysis. The resistivities were set with a greater error floor, equivalent to 5° in phase error, in an attempt to account for the final static shifts, or site gains, which are expected to be small (Groom and Bailey, 1989). A comparison of the models produced at 117° and at 108° revealed very little differences in major conductivity structures, indicating that the data are relatively insensitive to relatively small changes in geoelectric strike direction. Fig. 7a–d shows the derived four inversions of the distortion-corrected responses with a geoelectric strike direction of 108°. Full details of the inversion models can be found in Spratt (2003).

Although the shape and depth extent for many of the features varies between models, features A–E in Fig. 7 represent electrical structures that are found consistently whatever the choice of data. Inconsistencies which appear to be dependent on the choice of data will not be discussed herein. The normalized RMS misfits for these four models are 1.9 (TM-only), 3.5 (TM + GTF), 3.6 (TM + TE) and 4.4 (TM + TE + GTF), and the individual station RMS values are shown for the model of Fig. 7d in 9. Feature A is a shallow con-

ductive structure that extends to depths of ∼10 km at the southern end of the profile. Feature B is a slightly deeper conductor located south of the YZS, beginning at a depth of ∼10 km and extending to 20–30 km depth. Feature C is a northward-dipping conductor that may extend from the surface, south of the YZS, down to ∼30 km, north of the YZS. Above the base of feature C, feature D is a highly resistive structure near the surface north of the YZS. Finally there appears to be a southward dipping resistive structure, feature E, that separates the conductive regions B and C.
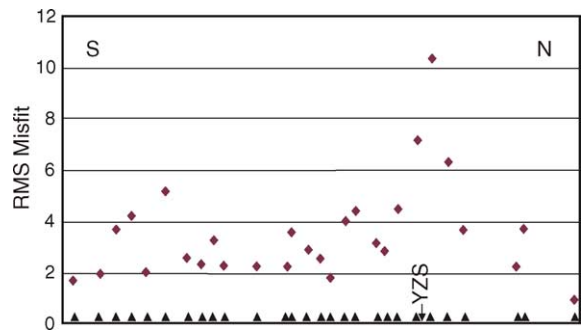

Fig. 9. Individual station RMS misfit for model shown in Fig. 7d that fits the TM, TE and GTF data.

Fig. 8 illustrates the consistencies between the pseudosections for the measured and calculated TM and TE responses of the data used in the TM + TE + GTF model (Fig. 7d), and the individual station misfit is shown in Fig. 9. The largest misfit is at the stations in the immediate vicinity of the Yarlung-Zanbgo suture, and is predominantly in the GTF data.

Beneath the Yarlung-Zanbgo suture, and extending northwards, phase increases with depth until ∼10,000 s where it drops to values below 60°. Although data coverage is sparse, this may be an indication of a more resistive layer at depth beneath the northern end of the profile.

5. Discussion and conclusions

First order observations of the modelled 700-line data indicate distinct conductive structures within the Tibetan crust in the vicinity of the Yarlung-Zangbo suture zone, which marks the surface expression of the India–Asia collision. There are several similarities between these structures and those seen in the modelled 100-line data along geoelectric-strike. We interpret these features in the following sections.

5.1. Feature A

A shallow conductive structure (<2 Ω m) that extends to ∼10 km depth. A similar along-strike feature has been observed and interpreted to represent sedimentary rocks from the Tethyan ocean that closed when India and Asia collided.

5.2. Feature B

A slightly deeper conductive structure (<2 Ω m) beginning at ∼10 km depth and extending to 20–30 km is apparent in each of the models. This feature may be associated with the along-strike feature of the 100-line model that has been attributed to ponded melt in the mid-upper crust.

5.3. Feature C

A northward dipping conductor beneath the Indus-Zangbo suture. A similar conductor, interpreted to represent partial melting of the mid-lower crust was re-

vealed in the 100-line profile, but, unlike the 100-line model, at this location the conductor appears to extend to close to the surface just south of the YZS. This may represent upward fluid migration within the crust.

5.4. Feature D

A highly resistive feature (>8000 Ω m) is revealed north of the Yarlung-Zangbo suture to depths of ∼20 km. This region feature, apparent in along-strike models, most likely represents the resistive Gangdese batholith on the Lhasa block of the Asian continent.

5.5. Feature E

Separating the two shallow conductors south of the Indus-Zangbo suture is a fairly resistive feature (∼500–1000 Ω m) dipping to the south. This resistive break between features B and C is required by all components the data, TE, TM and GTF. This perhaps is the most enigmatic result found to date and requires further elaboration. Clearly some process has occurred which has resulted in rocks with low permeability so that there is poor interconnection between potential conducting phases. Such a situation was also observed for the Eocene-aged Tintina fault in northwestern Canada (Ledo et al., 2002).

Further inversions of these data will be undertaken in an attempt to refine dimensions of the observed conductivity structures, in particular around the YZS. Model testing procedures will be applied to determine the validity of the discussed feature and to determine the depth of penetration of the data.

To date we have been unable to fulfil our primary ultra-long period objective, which was to penetrate below the conductor north of the YZS and determine the electrical nature of the deep crust and uppermost mantle. Further processing will take place to try to derive reliable estimates at the ultra-long periods.

period MT data. Reviews of an earlier version of this manuscript by Heinrich Brasse and Phil Wannamaker and the comments of Handling Editor Andreas Junge were all appreciated.

References

Berdichevsky, M.N., 1999. Marginal notes on magnetotellurics. Surv. Geophys. 20, 341–375.

Berdichevsky, M.N., Pokhotelov, D.O., 1997. Violation of the dispersion relations in a three-dimensional magnetotelluric model. Phys. Solid Earth 33, 603–612.

Besse, J., Courtillot, V., 1988. Paleogeographic maps of the continents bordering the Indian ocean since the Early Jurassic. J. Geophys. Res. 93, 11791–11808.

Brown, L.D., Zhao, W., Nelson, K.D., Hauck, M., Alsdorf, D., Ross, A., Cogan, M., Clark, M., Liu, X., Che, J., 1996. Bright spots, structure and magmatism in southern Tibet from INDEPTH seismic reflection profiling. Science 274, 1688–1690.

Chen, L., Booker, J.R., Jones, A.G., Wu, N., Unsworth, M.J., Wei, W., Tan, H., 1996. Electrically conductive crust in southern Tibet from INDEPTH magnetotelluric surveying. Science 274, 1694–1696.

Gamble, T.D., Goubau, W.M., Clarke, J., 1979. Magnetotellurics with a remote reference. Geophysics 44, 53–68.

Groom, R.W., Bailey, R.C., 1989. Decomposition of magnetotelluric impedance tensors in the presence of local three-dimensional galvanic distortion. J. Geophys. Res. 94, 1913–1925.

Jones, A.G., 1992. Electrical conductivity of the continental lower crust. In: Fountain, D.M., Arculus, R.J., Kay, R.W. (Eds.), Continental Lower Crust. Elsevier, Amsterdam, pp. 81–143, Chapter 3.

Jones, A.G., 1993. Electromagnetic images of modern and ancient subduction zones. In: Green, A.G., Kroner, A., Gotze, H.-J., Pavlenkova, N. (Eds.), Plate Tectonic Signatures in the Continental Lithosphere, Tectonophysics 219: 29–45.

Jones, A.G., 1999. Imaging the continental upper mantle using electromagnetic methods. Lithos 48, 57–80.

Jones, A.G., Jödicke, H., 1984. Magnetotelluric transfer function estimation improvement by a coherence-based rejection technique, Contributed Paper at 1984 Annual SEG Meeting, Atlanta, Georgia, USA. Abstract volume, pp. 51–55.

Jones, A.G., Chave, A.D., Egbert, G., Auld, D., Bahr, K., 1989. A comparison of techniques for magnetotelluric response function estimates. J. Geophys. Res. 94, 14201–14213.

Ledo, J., Jones, A.G., Ferguson, I.J., 2002. Electromagnetic images of a strike-slip fault: the Tintina Fault, northern Canadian Cordillera, Geophys. Res. Lett. 89 (8), doi: 10.1029/2001GL013408.

Li, S., Unsworth, M.J., Booker, J.R., Wei, W., Tan, H., Jones, A.G., 2003. Partial melt or aqueous fluid in the mid-crust of southern Tibet? Constraints from INDEPTH magnetotelluric data. Geophys. J. Int. 153, 289–304.

McNeice, G.W., Jones, A.G., 2001. Multisite, multifrequency tensor decomposition of magnetotelluric data. Geophysics 66, 158–173.

Mei, S., Kohlstedt, D.L., 2000. Influence of water on plastic deformation of olivine aggregates. 2. Dislocation creep regime. J. Geophys. Res. 105, 21471–21481.

Molnar, P., England, P., Martinod, J., 1993. Mantle dynamics, uplift of the Tibetan Plateau and the Indian monsoon. Rev. Geophys. 31, 357–396.

Nelson, K.D., Zhoa, W., Brown, L.D., Kuo, J., Che, J., Liu, X., Klemperer, S.L., Makovsky, Y., Meissner, R., Meckie, J., Kind, R., Wenzel, F., Ni, J., Nabelek, J., Leshou, C., Tan, H., Wei, W., Jones, A.G., Booker, J., Unsworth, M., Kidd, W.S.F., Hauck, M., Alsdorf, D., Ross, A., Cogan, M., Wu, C., Sandvol, E., Edwards, M., 1996. Partially molten middle crust beneath southern Tibet: synthesis of Project INDEPTH results. Science 274, 1684–1687.

Parker, R.L., Booker, J.R., 1996. Optimal one-dimensional inversion and bounding of magnetotelluric apparent resistivity and phase measurements. Phys. Earth Planet. Int. 98, 269–282.

Rodi, W., Mackie, R.L., 2001. Nonlinear conjugate gradients algorithm for 2-D magnetotelluric inversion. Geophysics 66, 174–187.

Spratt, J., 2003. Magnetotelluric investigation across the Yarlung-Zangbo suture zone, southern Tibet. M.Sc. Thesis, Syracuse University.

Wei, W., Unsworth, M., Jones, A.G., Booker, J., Tan, H., Nelson, D., Chen, L., Li, S., Solon, K., Bedrosian, P., Jin, S., Deng, M., Ledo, J., Kay, D., Roberts, B., 2001. Detection of widespread fluids in the Tibetan crust by magnetotelluric studies. Science 292, 716–718.

Weidelt, P., 1972. The inverse problem of geomagnetic induction. Z. Geophys. 38, 257–289.

Weidelt, P., Kaikkonen, P., 1994. Local 1-D interpretation of magnetotelluric B-polarization impedances. Geophys. J. Int. 117, 733–748.

Yin, A., Harrison, M., 2000. Geologic evolution of the Himalayan-Tibetan Orogen. Ann. Rev. Earth Planet. Sci. 28, 211–280.

Zhao, W., Nelson, K.D., and the Project INDEPTH Team, 1993. Project INDEPTH Team. Deep seismic reflection evidence for continental underthrusting beneath southern Tibet. Nature 366, 557–559.